Sensors & Diagnostics

PAPER

View Article Online
View Journal | View Issue

Cite this: *Sens. Diagn.*, 2023, **2**, 1302

A new detection mode for gold nanoparticle-linked immunosorbent assay (GNLISA) based on a clock reaction: instrument- and enzyme-free visual quantitative detection of prostate-specific antigen (PSA)†

Tianxiang Wu * and Xiao-Yuan Li

The enzyme-linked immunosorbent assay (ELISA) has been serving as both the workhorse and the gold standard in immunoassays due to its high specificity, sensitivity, and accuracy, despite its known shortcomings and limitations. In this work, we report our effort to improve the current ELISA protocol significantly by achieving the following four goals all together: first of all, we achieved enzyme-free signal generation in ELISA by replacing the conventional enzyme-based color generation step with an enzyme-free pure chemical color change process from a clock reaction. Secondly, we achieved the use of time lapse characteristically associated with a clock reaction as the quantitative readout signal for analyte concentration. Thirdly, gold nanoparticles (AuNPs) were employed for dual functions, both as a secondary antibody carrier and a catalytic regulator for the clock reaction. And last but not least, the clocking time associated with the colorimetric detection in our modified ELISA can be read out either by the naked eye assisted with a stopwatch free from any benchtop instrument or more accurately on any benchtop instrument with a built-in timer and with pre-set absorbance associated with the characteristic absorption wavelength of the clock reaction. The viability of our method is demonstrated by the quantitative detection of PSA in human serum and validated by both instrument-based measurements and commercial ELISA kits. The naked-eye detection range for PSA was found to be from 1.00 to 100 ng ml^{-1} with a limit of detection (LOD) of 0.96 ng ml^{-1}, which is lower than the typical threshold value (4 ng ml^{-1}), and a sensitivity of *ca.* 3.1 ng mL^{-1} min^{-1} for the early diagnosis of prostate cancer.

Received 20th March 2023,
Accepted 10th August 2023

DOI: 10.1039/d3sd00058c

rsc.li/sensors

1. Introduction

The enzyme-linked immunosorbent assay (ELISA) has been considered the gold standard in immunoassays due to its high specificity, sensitivity, and accuracy.[1] ELISA has found extensive applications in medical diagnosis,[2,3] immunology,[4,5] vaccine development,[4,6] toxicology,[7,8] drug monitoring and the pharmaceutical industry,[9,10] transplantation,[11,12] and the food industry,[13–15] among others. The conventional ELISA has been known to exhibit several shortcomings and limitations, including but not limited to (i) the tedious and laborious procedure, (ii) the lack of multiplexing options, (iii) the dependence on instruments for signal readout and quantitation, (iv) the requirement for a relatively high sample volume,[16] and (v) the need for skilled and trained operating personnel. Therefore, there have been extensive efforts to modify the current ELISA protocol with the aim of improving or even overcoming its shortcomings.[17–21] In the meantime, for its dominant applications in medical and clinical practices, the improvements on ELISA are expected to meet the World Health Organization (WHO)'s ASSURED requirements for bio-analytical platforms especially for the developing and under-developed areas, namely, (i) affordable, (ii) sensitive, (iii) specific, (iv) user-friendly, (v) rapid and robust, (vi) equipment-free, and (vii) deliverable to those in need for such technologies.[22]

The signal generation and readout in the conventional ELISA is often based on a colorimetric method consisting of two main steps.[23,24] The signal generation step employs an enzyme-based color change process of a chemical dye, while the signal readout and quantitation step often relies on a benchtop instrument to measure either absorbance or fluorescence.[25] The quantitative measurement by the naked eye, the most convenient, desirable and instrument-free detection, cannot be achieved and implemented on the

Department of Chemistry, The Hong Kong University of Science and Technology, Clear Water Bay, Kowloon, Hong Kong S.A.R, The People's Republic of China. E-mail: twuas@connect.ust.hk

† Electronic supplementary information (ESI) available. See DOI: https://doi.org/10.1039/d3sd00058c

conventional ELISA. On the other hand, metallic nanoparticles, especially Au and Ag nanoparticles, display substantial color changes when the nanoparticles' size, shape, or local environment changes associated with the changes of their localized surface plasmon resonance (LSPR).[26–28] There have been extensive reports on the use of various nanoparticles, especially gold nanoparticles (AuNPs) in ELISA to improve its signal generation and readout.[29] For example, ELISA combined with LSPR is named plasmonic ELISA (pELISA).[30] It appears that the more colors that can be read out in the concentration range comparable to that of the analyte, the higher the accuracy of the detection method when detected by the naked eye. By far, many multi-color detection schemes have been developed, including but not limited to wine red → colorless → yellow,[31] red → blue or blue → red,[32–35] blue → purple,[36] blue → mauve,[37] colorless → blue → red,[38] colorless → yellow,[39] and brownish → gray → cyan → green → blue → violet → red → colorless → yellow,[21] to name just a few. However, without exception, these reported efforts still rely on instruments for quantitative detection. Recently, Qin's group reported a ruler-based method that reads the height associated with the air pressure in a modified ELISA to achieve enzyme-free and visual quantitative detection.[19,20,40,41]

Clock reactions belong to a special class of reactions that have been known for more than a century.[42] The definition of a clock reaction is a system presenting an induction period (well-defined time lag) followed by an abrupt change in the concentration of some chemical species participating in the reaction. One unique feature of certain clock reactions is that it allows the establishment of quantitative relationships between the induction time (or clocking time) and the concentration of involved chemical species. The quantitative readout of time lapse requires only a stopwatch, offering a quantitative analytical method free from any benchtop instrument. In addition, certain clock reactions are known to involve the color change of reacting species, making them viable choices for quantitative detection *via* visual colorimetry. The use of clock reactions in quantitative chemical and biochemical detection has been rare.[43–45] There were two clock reaction-based immunoassays to achieve instrument-free visual quantitative detection. The first work was reported in 1987, and the height of the chromogenic substance was used as the readout signal for detection.[46] The second work was reported in 1997 where the time lapse was used as the readout signal for detection.[47] However, both studies still utilized enzymes in their detection protocol. In this work, we report the combination of a modified ELISA (gold nanoparticle-linked immunosorbent assay or GNLISA) with a clock reaction to achieve instrument- and enzyme-free visual quantitative detection of prostate-specific antigen (PSA).

2. Experimental section

2.1 Materials

Gold(III) chloride trihydrate ($HAuCl_4{\cdot}3H_2O$), hexadecyltrimethylammonium bromide (CTAB), sodium borohydride ($NaBH_4$, powder), methylene blue (MB^+, chloride salt), mercury(II) chloride, cadmium(II) chloride, lead(II) chloride, iron(III) chloride, di-sodium hydrogen phosphate dihydrate ($Na_2HPO_4{\cdot}2H_2O$), potassium phosphate monobasic (KH_2PO_4), sodium chloride (NaCl), potassium chloride (KCl), Tween 20, bovine serum albumin (BSA), and human serum were all from Sigma Aldrich and were used as received without further purification. Sodium citrate (Fisher Scientific), sodium thiosulfate solution (Fluka), coating prostate-specific antibodies (Monoclonal, Linc-Bio), prostate-specific antigen (Linc-Bio), labeling prostate-specific antibodies (Monoclonal, Linc-Bio), and a human kallikrein 3/PSA Quantikine ELISA kit (R&D System) were purchased from respective suppliers and were used without any further treatment.

2.2 Instruments

All UV-vis absorption spectra were recorded on a UV-1800 spectrometer (Shimadzu, Japan). All cycle times of clock reaction were recorded using a stopwatch. The morphology and size distribution of the as-prepared AuNPs were measured with a JEOL 2010F analytical transmission electron microscope (TEM). Ultrapure deionized water from a NANOpure (Barnstead) source was used throughout the experiments. A microplate reader (Thermo Scientific) was used when using the commercial ELISA kits for antigen detection. Excessive labeling antibodies not modified on the AuNPs were removed using a centrifuge 5418 R (Eppendorf). The measurements were conducted at room temperature of 22 °C, while the constant temperature condition of 37 °C for certain steps was obtained on an incubator (Memmert).

2.3 Preparation and characterization of AuNPs

The preparation of AuNPs was based on the well-established method using citrate reduction of $HAuCl_4$ in water.[48] Briefly, a 72.7 mL aqueous solution of 1 mmol L^{-1} $HAuCl_4$ was added into a round-bottom flask equipped with a reflux condenser and then heated to boil under gentle stirring. 38.8 mmol L^{-1} sodium citrate (7.3 mL) was added rapidly to the solution. The solution was heated under reflux for another 15 min. The color changed from pale yellow to deep red. The solution was stirred continuously and cooled down to room temperature. Finally, the AuNPs were obtained and stored at 4 °C for further use. The as-prepared AuNPs were analyzed with TEM. As can be seen from the TEM image (Fig. S1†), the as-synthesized AuNPs are quite uniform in size and shape with an average size of *ca.* 13 nm.

2.4 Preparation of the washing and blocking buffers

Washing buffer: 0.20 g KH_2PO_4, 1.44 g $Na_2HPO_4{\cdot}2H_2O$, 8.00 g NaCl, 0.20 g KCl, and 0.5 mL Tween 20 were dissolved in ultrapure deionized water. Then, the solution was transferred into a 1000 ml volumetric flask, and ultrapure water was added to 1000 ml.

Blocking buffer: 2.00 g BSA was dissolved in 100 ml washing buffer.

2.5 Preparation of AuNPs loaded with the labeling antibodies

55 μL of 0.20 M NaOH was added into 5.0 mL of 3.0 nM AuNPs under stirring at 400 rpm. 50 μL of 1 mg mL^{-1} labeling antibody was then added into the mixture at room temperature and kept still for 30 min. The as-prepared mixture was then centrifuged at 13 000 rpm at 4 °C for 30 min. After that, 4.1 mL supernatant was discarded, and 100 μL of 10% BSA solution was added into the mixture to incubate at room temperature for 30 min. After the incubation, 4.4 mL washing buffer was added to the mixture and centrifuged at 13 000 rpm at 4 °C for 30 min (this process was repeated three times). Finally, the precipitate was re-dissolved in 5.0 mL washing buffer and stored in a 4 °C refrigerator for further use.

2.6 The procedure of GNLISA for PSA detection

1 mg mL^{-1} coating antibody was diluted 200 times with 50 mM bicarbonate of pH 9.60 to obtain 5 μg mL^{-1} coating antibody solution. Then, 100 μL of 5 μg mL^{-1} coating antibody solution was added into the wells of a 96-well plate and incubated at 4 °C overnight. After removing the coating antibody, the plate wells were washed three times by filling the wells with 300 μL washing buffer. 200 μL blocking buffer was then added into the plate wells to block the remaining protein binding site for 2 h at room temperature. After three times washing with 300 μL washing buffer, 100 μL of different concentrations of PSA antigen were added into each well. After 1 hour incubation at 37 °C, the plate wells were washed three times with 300 μL washing buffer. 100 μL AuNPs loaded with the labeling antibodies were added to each well and the plate was incubated for 1 hour at 37 °C. After three times washing with 300 μL washing buffer, the plate wells were washed with ultrapure water three times as well. 75 μL of pH 7.96 Britton–Robinson buffer (B–R buffer), 10 μL of 0.10 M $Na_2S_2O_3$, 10 μL of 1 μM Cd^{2+}, 5 μL of 0.10 M CTAB, and 3.5 μL of 0.45 mM MB^+ were added into each well for 40 min to leach the AuNPs into $Au(S_2O_3)_2^{3-}$. Then, 20 μL of ω = 1.00% $NaBH_4$, was added to the plate wells, and the timer was then started. After the color changed from navy blue to colorless and back to light blue (0.68 μM MB^+, absorbance was at *ca.* 0.05), the timer was stopped to record the cycle time.

3. Results and discussion

3.1 The procedure of the method

Fig. 1 shows the mechanism of the proposed GNLISA and clock reaction for the instrument- and enzyme-free visual quantitative detection of PSA. Briefly, a typical sandwich-type ELISA is used and further modified. The coating antibody immobilized on the surface of the wells of a 96-well plate was utilized for the capture of the antigen. Next, AuNPs loaded with the labeling antibodies were combined with the antigen to form an antibody–antigen–second antibody sandwich complex on the well surface. The AuNP leaching reaction in the scheme is given below:

$$\text{Leaching Reaction: } 4Au + 8S_2O_3^{2-} + O_2 + 2H_2O \rightarrow 4[Au(S_2O_3)_2]^{3-} + 4OH^-$$

The AuNPs attached to the plate-well surface were leached to form $Au(S_2O_3)_2^{3-}$. A higher concentration of antigen leads to a higher concentration of $Au(S_2O_3)_2^{3-}$. The next step was the signal readout process. A clock reaction was used to distinguish the different concentrations of $Au(S_2O_3)_2^{3-}$ achieved by the GNLISA and leaching reaction. After $NaBH_4$ was added, both $Au(S_2O_3)_2^{3-}$ and Cd^{2+} were reduced to form Au_x/Cd_y nanoalloy particles, which could catalyze both the oxidation of $NaBH_4$ by the dissolved oxygen and the reduction of MB^+ (blue color) to form reduced MB^+ (colorless). During the process, the color of the solution changes from blue to colorless. With the hydrolysis of $NaBH_4$, the reduced MB^+ will be re-oxidized back to MB^+ by the oxygen diffused into and dissolved in the solution. This process is accompanied by the color change from colorless back to blue. Different concentrations of $Au(S_2O_3)_2^{3-}$ would lead to different times for the color to change from blue to

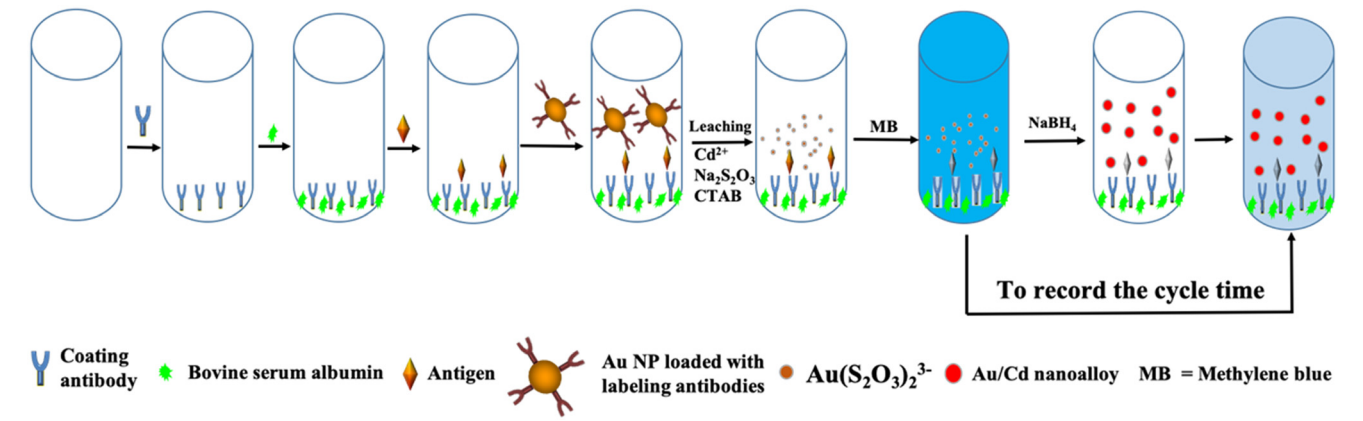

Fig. 1 Scheme of detection of PSA based on the GNLISA and clock reaction.

colorless and back to blue. We defined this time as the cycle time. More $Au(S_2O_3)_2^{3-}$ would result in a longer cycle time. The reason is that a higher concentration of $Au(S_2O_3)_2^{3-}$ would give rise to a higher concentration of Au_x/Cd_y nanoalloy particles, which in turn leads to a longer cycle time, and the rate of oxygen consumption in solution is faster than that of oxygen dissolution in solution, and that the rate of MB^+ reduction is faster than the rate of oxidation of the reduced MB^+.[49] The concentration of antigen is quantitatively correlated to the concentration of $Au(S_2O_3)_2^{3-}$, and in turn to the cycle time.

3.2 Optimization of the key assay conditions

When the concentration of $Na_2S_2O_3$ is lower than 0.05 M after $NaBH_4$ is added, the color cannot become colorless, or the time for the color to become colorless is too long (at least 6 min) to be applied as a cycle time for 100 ng ml^{-1} PSA. As for 0 ng ml^{-1} PSA, when the concentration of $Na_2S_2O_3$ is lower than 0.1 M, it shows the same phenomenon. As shown in Fig. 2A, when the concentration of $Na_2S_2O_3$ is in the range from 0.05 to 1.00 M for 100 ng ml^{-1} PSA, the cycle time is positively correlated with the concentration of $Na_2S_2O_3$. For 0 ng ml^{-1} PSA, the same phenomenon occurs in the concentration range from 0.10 M to 1.00 M. Due to the higher concentration of $Na_2S_2O_3$, more AuNPs will be leached into $Au(S_2O_3)_2^{3-}$ in 40 min leaching time, which results in a higher concentration of Au_x/Pb_y nanoalloy. The higher concentration of Au_x/Pb_y nanoalloy leads to a longer cycle time. Finally, 0.10 M $Na_2S_2O_3$ was selected for the experiment after considering the sensitivity (the cycle time difference between 0 and 100 ng ml^{-1} PSA antigen divided by (100–0) ng ml^{-1}) and effectiveness (the length of cycle time and leaching time).

Since it has been reported that some metal ions will accelerate the leaching reaction, and different Au_x/M_y nanoalloys show different effects on the catalytic clock reaction, we used Pb^{2+} ions (Cd^{2+} ions display a similar trend but higher activity) when optimizing the leaching time.[45,50–53] As shown in Fig. 2B, the cycle times for 0 and 100 ng ml^{-1} PSA are both positively correlated with

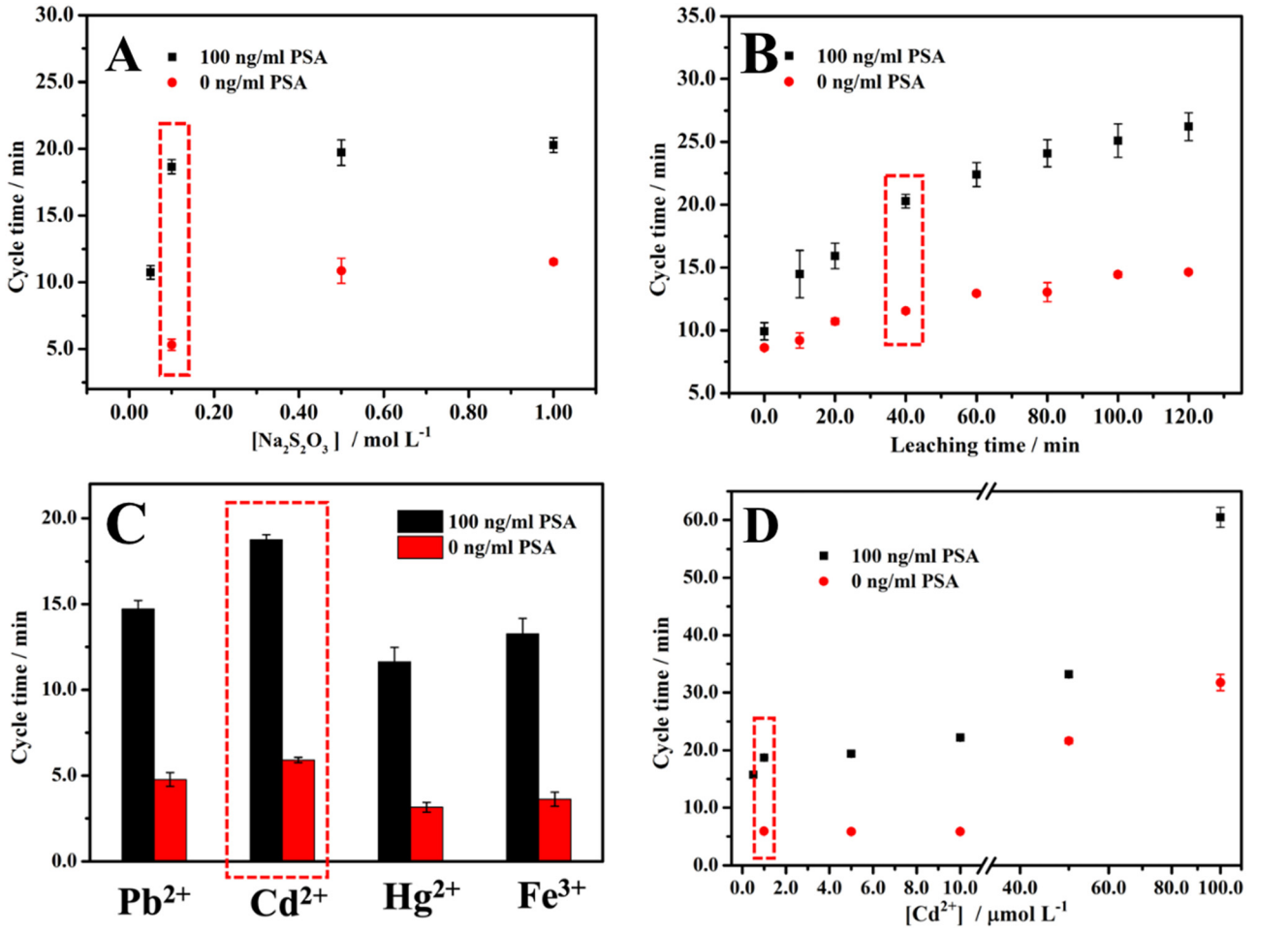

Fig. 2 The effect of (A) the concentration of the leaching agent $Na_2S_2O_3$, (B) the leaching time of AuNPs, (C) the different AuNP passivating metal ions at 1 μM concentration, and (D) Cd^{2+} at different concentrations on the cycle time. See text for the detailed conditions.

the leaching time. According to the scheme of the method, the cycle time for 0 ng ml^{-1} PSA is unrelated to the leaching time, which is inconsistent with the result. The possible reason is the non-specific adsorption of the AuNPs loaded with the labeling antibodies. The reason for the positive correlation between the cycle time and the leaching time is that a longer leaching time means that more AuNPs will be leached to produce more $Au(S_2O_3)_2^{3-}$, thereby leading to a higher concentration of Au_x/Pb_y nanoalloy particles. Considering the balance between sensitivity and effectiveness in the measurements, we chose 40 min leaching time for all the experiments in measuring PSA.

It was reported that the leaching reaction could be accelerated in the presence of Pb^{2+} or other divalent metal ions.[50–53] The effect of the concentration of Pb^{2+} on the cycle time was explored (Fig. S2†). When the concentration of Pb^{2+} is lower than 0.50 μM after $NaBH_4$ is added, either the color of the solution remains unchanged or the time for the color to become colorless is too long (>6 min) to be practically used as a cycle time for 100 ng ml^{-1} PSA. As for 0 ng ml^{-1} PSA, when the concentration of Pb^{2+} is lower than 1.0 μM, the same phenomenon occurs. As shown in Fig. S2,† when the concentration of Pb^{2+} was in the range from 0.50 to 100 μM for 100 ng ml^{-1} PSA, the cycle time was in a positive correlation with the concentration of Pb^{2+}. When the Pb^{2+} concentration was in the range from 1.0 to 100 μM, the same relationship between the cycle time and the concentration of Pb^{2+} was obtained for 0 ng ml^{-1} PSA. This is because the higher the concentration of Pb^{2+}, the more AuNPs will be leached into $Au(S_2O_3)_2^{3-}$, resulting in a higher concentration of Au_x/Pb_y nanoalloy particles. The higher Au_x/Pb_y nanoalloy particle concentration would result in a longer cycle time. We chose 1.0 μM Pb^{2+} concentration as the optimal experiment condition considering the balance between the sensitivity and effectiveness.

Different metal ions have different effects on the leaching and catalytic reactions by forming different types of Au_x/M_y nanoalloy particles. It has been shown that Pb^{2+}, Cd^{2+}, Hg^{2+}, and Fe^{3+} all have a noticeable effect on the cycle time.[40] Therefore, the effects of Pb^{2+}, Cd^{2+}, Hg^{2+}, and Fe^{3+} at a concentration of 1.0 μM on the cycle time were comparatively studied and the results are shown in Fig. 2C. Since Cd^{2+} is more relatively less toxic than Pb^{2+}, the effect of Cd^{2+} at different concentrations on the cycle time was also studied and the results are shown in Fig. 2D. Balancing all the considerations, we selected Cd^{2+} at 1.0 μM concentration for the following experiments.

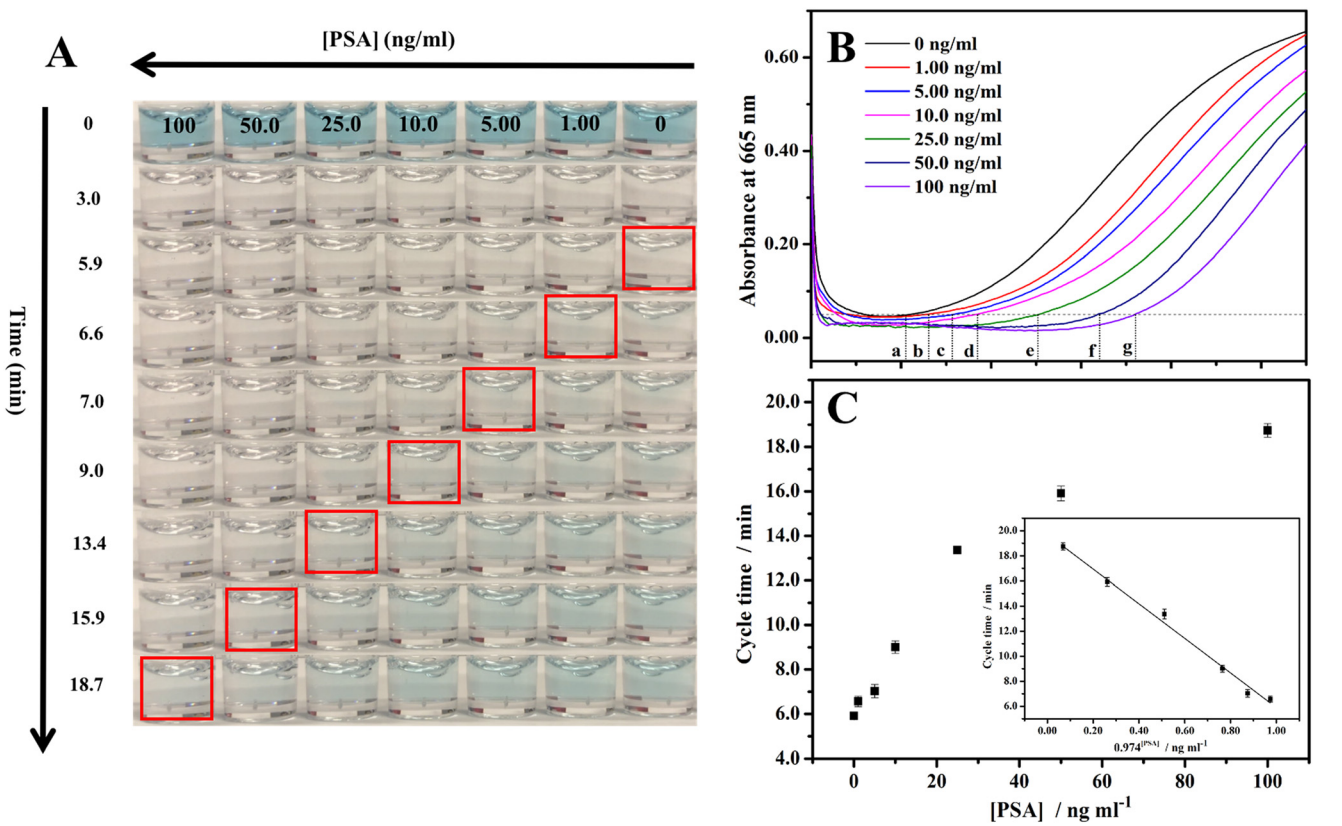

Fig. 3 (A) The times of color change of MB^+ in the clock reaction for different concentrations of PSA, (B) the changes of absorbance at 665 nm (a characteristic peak of MB^+) with time for different concentrations of PSA. The points at a–g denote the times when the absorbance at 665 nm is 0.05, and (C) the corresponding plot of time observed by the naked eye *vs.* the concentration of PSA. Inset: calibration plot of PSA.

3.3 Instrument-free visual quantitative detection of PSA

Quantitative PSA detection using time lapse as the readout both by the naked eye/stopwatch (Fig. 3A) and on a benchtop UV-vis spectrophotometer (Fig. 3B) was conducted. The video of the color change corresponding to different concentrations of PSA is shown as Video S1 in the ESI.† The cycle times were 5.9, 6.6, 7.0, 9.0, 13.4, 15.9, and 18.7 min with the naked eye for 0, 1.00, 5.00, 10.0, 25.0, 50.0, and 100 ng ml^{-1} PSA, respectively. For the same set of samples with the measurements on a UV-vis spectrophotometer in time mode at the absorbance of 0.05, the cycle times were 5.5, 6.3, 7.9, 9.2, 13.1, 15.9, and 18.8 min, respectively, in quite good consistency with the cycle times obtained by the naked eye/stopwatch method (Fig. 3A). This demonstrates that the cycle times observed with the naked eye are reliable. The limit of detection (LOD: the PSA concentration corresponding to a signal that is three times the standard deviation above the zero calibrator) of this assay was measured, where the concentration of PSA was increased from 0 to 100 ng ml^{-1} and the cycle time ranged from 5.9 to 18.7 min. The calibration curve of the cycle time against the PSA concentration was linear from 1 to 100 ng ml^{-1} (r^2 = 0.992, n = 3) with a LOD of 0.96 ng ml^{-1} (Fig. 3C). The threshold value was 4 ng ml^{-1} for the early diagnosis of prostate cancer,[54] indicating that this method, when optimized, can be employed in the early diagnosis of prostate cancer. We also explored the cycle times observed by different observers and the results are listed in Table S1.† Different observers did show variation in the judgment of the endpoint color, and the typical deviation is less than 0.7 min. Table S2† summarizes the advantages (instrument- and enzyme-free visual quantitative detection) of this method in comparison with other reported methods. The relevant literature studies are also given in the ESI.†

3.4 Selectivity of the method

The selectivity of our GNLISA method in the PSA detection was examined and is shown in Fig. 4. We investigated the cycle times in the presence of various possible interferents and then compared them with the cycle time for PSA alone, including uric acid (UA), glucose, ascorbic acid (AA), immunoglobulin G (IgG), carcinoembryonic antigen (CEA), and alpha-fetoprotein (AFP). We also studied the cycle time of PSA mixed with interferents and then compared it with the cycle time for PSA alone. Fig. 4A shows the colors of 1000 ng ml^{-1} interfering substances and 25 ng ml^{-1} PSA after 0, 3.0, 6.5, and 13.5 min of reaction. The corresponding observed cycle times are listed in Fig. 4B and Table S3.† In the presence of an interfering substance at a concentration 40 times that of PSA, the cycle time did not show appreciable change. These results illustrate that the presence of individual interfering substances does not affect the PSA detection. To further illustrate the high selectivity of this method, we also explored a set of binary systems and

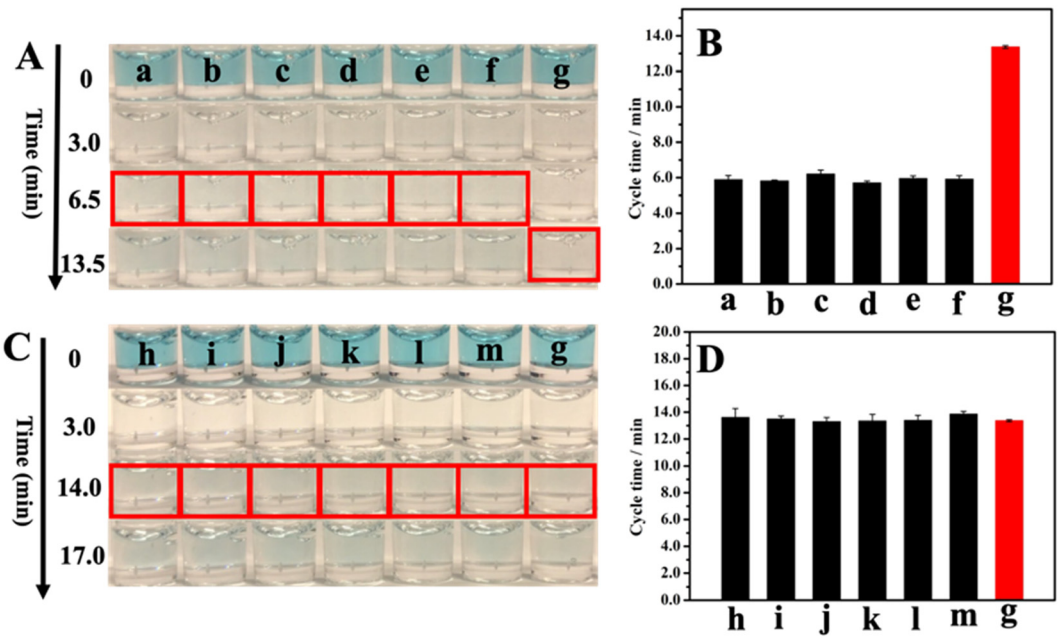

Fig. 4 (A) The color changes of MB^+ in the clock reaction along with time for 1000 ng ml^{-1} UA (a), 1000 ng ml^{-1} glucose (b), 1000 ng ml^{-1} AA (c), 1000 ng ml^{-1} IgG (d), 1000 ng ml^{-1} CEA (e), 1000 ng ml^{-1} AFP (f), and 25 ng ml^{-1} PSA (g). (B) Histogram of the cycle time towards 1000 ng ml^{-1} UA (a), 1000 ng ml^{-1} glucose (b), 1000 ng ml^{-1} AA (c), 1000 ng ml^{-1} IgG (d), 1000 ng ml^{-1} CEA (e), 1000 ng ml^{-1} AFP (f), and 25 ng ml^{-1} PSA (g). (C) 1000 ng ml^{-1} UA + 25 ng ml^{-1} PSA (h), 1000 ng ml^{-1} glucose + 25 ng ml^{-1} PSA (i), 1000 ng ml^{-1} AA + 25 ng ml^{-1} PSA (j), 1000 ng ml^{-1} IgG + 25 ng ml^{-1} PSA (k), 1000 ng ml^{-1} CEA + 25 ng ml^{-1} PSA (l), 1000 ng ml^{-1} AFP + 25 ng ml^{-1} PSA (m), and 25 ng ml^{-1} PSA (g). (D) Histogram of the cycle time towards 1000 ng ml^{-1} UA + 25 ng ml^{-1} PSA (h), 1000 ng ml^{-1} glucose + 25 ng ml^{-1} PSA (i), 1000 ng ml^{-1} AA + 25 ng ml^{-1} PSA (j), 1000 ng ml^{-1} IgG + 25 ng ml^{-1} PSA (k), 1000 ng ml^{-1} CEA + 25 ng ml^{-1} PSA (l), 1000 ng ml^{-1} AFP + 25 ng ml^{-1} PSA (m), and 25 ng ml^{-1} PSA (g).

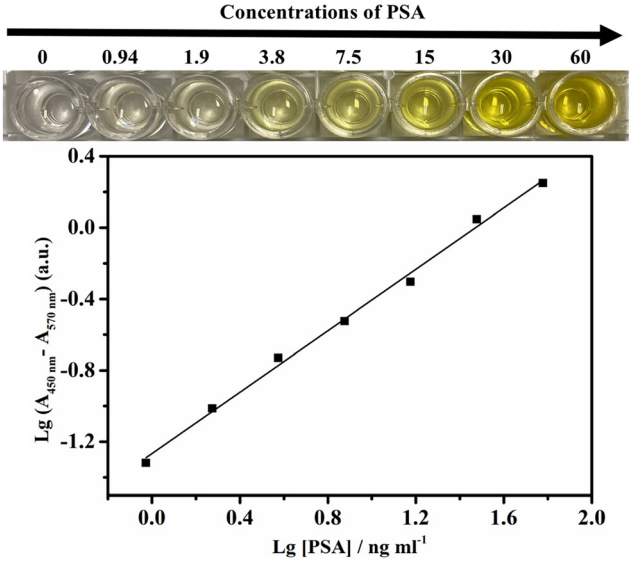

Fig. 5 The top photograph shows the detection of PSA in different concentrations using the commercial ELISA kit. The bottom graph is the calibration curve employing a set of standard solutions with known PSA concentrations.

compared the cycle time for PSA alone with the cycle time for PSA mixed with individual interfering substances. The results are listed in Fig. 4C and D, and Table S3,† respectively. Fig. 4C shows the colors of 25 ng ml^{-1} PSA and 25 ng ml^{-1} PSA + 1000 ng ml^{-1} interfering substances after 0, 3.0, 14.0, and 17.0 minutes of reaction. Fig. 4D and Table S3† show the cycle times for 25 ng ml^{-1} PSA and 25 ng ml^{-1} PSA + 1000 ng ml^{-1} interfering substances. The cycle times for 25 ng ml^{-1} PSA in the absence and presence of a 1000 ng ml^{-1} interfering substance are very close to each other, demonstrating that even the coexistence of interfering substances at a concentration of 40 times higher than that of PSA will not affect the test results. Put together, these results demonstrate that our method has a high selectivity.

3.5 Validation of this method by the commercial ELISA kit for the PSA detection

After having obtained the standard calibration curve and confirmed the high selectivity of this method, to demonstrate its viability in actual applications, we used the method to detect PSA in human serum and compared the results with those obtained from the commercial ELISA kit method. The standard curve of the commercial ELISA kit was measured first and is shown in Fig. 5. The PSA in human serum samples and human serum alone (the blank) was detected by our method. The results from our method and those from the commercial ELISA kit are listed in Table 1. The recovery is in the range of 85.3% to 96.9%, demonstrating that our method is viable in potential applications in the detection of PSA in human serum. The typical assay times of the commercial ELISA kit and this method are comparable, depending on the concentration range of PSA.

It should be pointed out, however, that this method has its own drawbacks and limitations for further improvement. For example, the clocking time of the employed clock reaction is intrinsically dependent on both the temperature (Fig. S3†) and the oxygen partial pressure of the atmosphere. This would eventually require an optimized and facile calibration protocol for viable applications in underdeveloped areas. The use of a relatively time-consuming leaching reaction is another issue calling for further improvement. Last but not least is the desire to replace cadmium ions with other less toxic ions such as Fe(III) or Cu(II). Future work may focus on solving or improving these limitations.

4. Conclusion

In conclusion, we report the development of a new mode of detection to significantly improve the current ELISA protocol. Our method has four main features. First of all, we achieved enzyme-free signal generation in ELISA by replacing the conventional enzyme-based color generation step with an enzyme-free pure chemical color change process from a clock reaction. Secondly, we achieved the use of the clocking time characteristically associated with a clock reaction as the quantitative readout signal for analyte concentration. Thirdly, AuNPs were employed for dual functions, both as a secondary antibody carrier and a catalytic regulator for the clock reaction. And last but not least, the characteristic time associated with the colorimetric detection in our modified ELISA can be read out either by the naked eye assisted with a stopwatch free from any benchtop instrument or more accurately on any benchtop instrument with a built-in timer and with pre-set absorbance associated with the characteristic absorption wavelength of the clock reaction. The feasibility of our method is demonstrated by the quantitative detection of PSA in human serum and validated by both instrument-based measurements and commercial

Table 1 Comparison of this method with the commercial ELISA kit

Added (ng ml^{-1})	Found by the commercial ELISA kit (ng ml^{-1})	Standard deviation for the commercial ELISA kit	Found by this method (ng ml^{-1})	Standard deviation for this method	Recovery (%)
0	0.914	0.0150	0.850	0.130	93.0
1	1.09	0.151	0.960	0.174	88.1
4	4.98	0.233	4.25	0.328	85.3
10	11.9	0.325	11.4	0.435	95.8
60	58.2	0.268	56.4	0.816	96.9

ELISA kits. The naked-eye detection range for PSA is from 1.00 to 100 ng ml^{-1} with a LOD of 0.96 ng ml^{-1}, which is lower than the threshold value (4 ng ml^{-1}) for the early diagnosis of prostate cancer.

Conflicts of interest

The authors declare that they have no known competing financial interests or personal relationships that could have appeared to influence the work reported in this paper.

Acknowledgements

This research was supported by the Department of Chemistry of HKUST and the Grant from Research Grant Council of Hong Kong (No. 16307721).

References

1 S. Hosseini, P. Vázquez-Villegas, M. Rito-Palomares and S. O. Martinez-Chapa, *Enzyme-linked Immunosorbent Assay (ELISA) From A to Z*, Springer Singapore, Singapore, 2018.
2 J. N. Roberts, T. M. Byrem and D. L. Grooms, *Reprod. Domest. Anim.*, 2015, **50**, 651–658.
3 H. Ye, K. Yang, J. Tao, Y. Liu, Q. Zhang, S. Habibi, Z. Nie and X. Xia, *ACS Nano*, 2017, **11**, 2052–2059.
4 N. Sharma, S. Hanif, D. Upadhyay and M. K. Chhikara, *J. Immunol. Methods*, 2019, **473**, 112634–112640.
5 G. Mameli, D. Cossu, E. Cocco, J. Frau, M. G. Marrosu, M. Niegowska and L. A. Sechi, *J. Neuroimmunol.*, 2015, **280**, 66–68.
6 Q. Pan, J. Wang, Y. Gao, H. Cui, C. Liu, X. Qi, Y. Zhang, Y. Wang, K. Li, L. Gao and X. Wang, *Appl. Microbiol. Biotechnol.*, 2020, **104**, 853–859.
7 Y. Xiong, K. Pei, Y. Wu and Y. Xiong, *Food Control*, 2017, **78**, 317–323.
8 M. Laloup, G. Tilman, V. Maes, G. De Boeck, P. Wallemacq, J. Ramaekers and N. Samyn, *Forensic Sci. Int.*, 2005, **153**, 29–37.
9 B. D. Hock, L. K. Stamp, M. W. Hayman, P. E. Keating, E. T. Helms and M. L. Barclay, *Ther. Drug Monit.*, 2016, **38**, 32–41.
10 E. M. H. Schmitz, D. Kerkhof, D. Hamann, J. L. Dongen, P. H. M. Kuijper, L. Brunsveld, V. Scharnhorst and M. A. C. Broeren, *Clin. Chem. Lab. Med.*, 2016, **54**, 1211–1219.
11 M. H. L. Christiaans, F. Nieman, J. P. Hooff and E. M. Berg-Loonen, *Transplantation*, 2000, **69**, 917–927.
12 G. Fernández-Fresnedo, J. M. Pastor, M. López-Hoyos, J. C. Ruiz, J. A. Zubimendi, J. Gonzalez-Cotorruelo, E. Rodrigo, A. L. M. Francisco and M. Arias, *Nephrol., Dial., Transplant.*, 2003, **18**, 990–995.
13 B. Mariager, M. Sølve, M. Eriksen and C. H. Brogren, *Food Agric. Immunol.*, 1994, **6**, 73–83.
14 X. Jiang, Q. Rao, K. Mittl and Y. H. P. Hsieh, *Food Control*, 2020, **110**, 107045–107052.
15 K. O. Ivens, J. L. Baumert and S. L. Taylor, *J. Food Sci.*, 2016, **81**, T1871–T1878.
16 Ref. 1, pp. 68–69.
17 H. D. Hill and C. A. Mirkin, *Nat. Protoc.*, 2006, **1**, 324–336.
18 S. I. Stoeva, J. S. Lee, C. S. Thaxton and C. A. Mirkin, *Angew. Chem., Int. Ed.*, 2006, **45**, 3303–3306.
19 Y. Li, J. Xuan, Y. Song, W. Qi, B. He, P. Wang and L. Qin, *ACS Nano*, 2016, **10**, 1640–1647.
20 Y. Song, X. Xia, X. Wu, P. Wang and L. Qin, *Angew. Chem., Int. Ed.*, 2014, **53**, 12451–12455.
21 X. Ma, Z. Chen, P. Kannan, Z. Lin, B. Qiu and L. Guo, *Anal. Chem.*, 2016, **88**, 3227–3234.
22 M. Urdea, L. A. Penny, S. S. Olmsted, M. Y. Giovanni, P. Kaspar, A. Shepherd, P. Wilson, C. A. Dahl, S. Buchsbaum, G. Moeller and D. C. Hay Burgess, *Nature*, 2006, **444**, 73–79.
23 Z. Yu, H. Gong, M. Li and D. Tang, *Biosens. Bioelectron.*, 2022, **218**, 114751–114759.
24 R. Ren, G. Cai, Z. Yu, Y. Zeng and D. Tang, *Anal. Chem.*, 2018, **90**, 11099–11105.
25 P. Peng, C. Liu, Z. Li, Z. Xue, P. Mao, J. Hu, F. Xu, C. Yao and M. You, *TrAC, Trends Anal. Chem.*, 2022, **152**, 116605–116617.
26 E. Petryayeva and U. J. Krull, *Anal. Chim. Acta*, 2011, **706**, 8–24.
27 G. Cai, Z. Yu, R. Ren and D. Tang, *ACS Sens.*, 2018, **3**, 632–639.
28 S. Lv, K. Zhang, Q. Zhou and D. Tang, *Sens. Actuators, B*, 2020, **310**, 127874–127880.
29 M. S. Tabatabaei, R. Islam and M. Ahmed, *Anal. Chim. Acta*, 2021, **1143**, 250–266.
30 J. Satija, N. Punjabi, D. Mishra and S. Mukherji, *RSC Adv.*, 2016, **6**, 85440–85456.
31 L. Guo, S. Xu, X. Ma, B. Qiu, Z. Lin and G. Chen, *Sci. Rep.*, 2016, **6**, 1–7.
32 Z. Zhang, Z. Chen, S. Wang, F. Cheng and L. Chen, *ACS Appl. Mater. Interfaces*, 2015, **7**, 27639–27645.
33 D. Cecchin, R. De La Rica, R. E. S. Bain, M. W. Finnis, M. M. Stevens and G. Battaglia, *Nanoscale*, 2014, **6**, 9559–9562.
34 R. De La Rica and M. M. Stevens, *Nat. Nanotechnol.*, 2012, **7**, 821–824.
35 R. De La Rica and M. M. Stevens, *Nat. Protoc.*, 2013, **8**, 1759–1764.
36 J. Liang, C. Yao, X. Li, Z. Wu, C. Huang, Q. Fu, C. Lan, D. Cao and Y. Tang, *Biosens. Bioelectron.*, 2015, **69**, 128–134.
37 C. Yao, S. Yu, X. Li, Z. Wu, J. Liang, Q. Fu, W. Xiao, T. Jiang and Y. Tang, *Anal. Bioanal. Chem.*, 2017, **409**, 1093–1100.
38 X. Huang, R. Chen, H. Xu and W. Lai, *Anal. Chem.*, 2016, **88**, 1951–1958.
39 Z. Xuan, M. Li, P. Rong, W. Wang, Y. Li and D. Liu, *Nanoscale*, 2016, **8**, 17271–17277.
40 Y. Song, Y. Zhang, P. E. Bernard, J. M. Reuben, N. T. Ueno, R. B. Arlinghaus, Y. Zu and L. Qin, *Nat. Commun.*, 2012, **3**, 1–9.
41 Y. Li, J. Xuan, T. Xia, X. Han, Y. Song, Z. Cao, X. Jiang, Y. Guo, P. Wang and L. Qin, *Anal. Chem.*, 2015, **87**, 3771–3777.
42 A. K. Horváth and I. Nagypál, *ChemPhysChem*, 2015, **16**, 588–594.
43 L. Zheng, H. Yu, Y. Yue, F. Wu and Y. He, *ACS Appl. Mater. Interfaces*, 2017, **9**, 11798–11802.
44 T. Wu and Z. Ma, *Microchim. Acta*, 2017, **184**, 577–582.
45 T. Wu, J. Shan and Z. Ma, *ACS Sustainable Chem. Eng.*, 2017, **5**, 4976–4981.

46 R. Chen, T. M. Li, H. Merrick, R. F. Parrish, V. Bruno, A. Kwong, C. Stiso and D. J. Litman, *Clin. Chem.*, 1987, **33**, 1521–1525.
47 R. Muller, *Biotechnol. Appl. Biochem.*, 1997, **26**, 73–78.
48 J. Turkevich, P. C. Stevenson and J. Hillier, *Discuss. Faraday Soc.*, 1951, **11**, 55–75.
49 T. Wu and X. Y. Li, *Anal. Methods*, 2023, **15**, 48–55.
50 X. Fu, T. Lou, Z. Chen, M. Lin, W. Feng and L. Chen, *ACS Appl. Mater. Interfaces*, 2012, **4**, 1080–1086.
51 Y. Y. Chen, H. T. Chang, Y. C. Shiang, Y. L. Hung, C. K. Chiang and C. C. Huang, *Anal. Chem.*, 2009, **81**, 9433–9439.
52 G. Deschenes, R. Lastra, J. R. Brown, S. Jin, O. May and E. Ghali, *Miner. Eng.*, 2000, **13**, 1263–1279.
53 D. Feng and J. S. J. Van Deventer, *Hydrometallurgy*, 2002, **64**, 231–246.
54 D. A. Healy, C. J. Hayes, P. Leonard, L. McKenna and R. O'Kennedy, *Trends Biotechnol.*, 2007, **25**, 125–131.